Düzce University
Journal of Science & Technology

Research Article

Surface Analysis of Magnesium AZ31 Samples Immersed in Various Aqueous Solutions

Erdem Şahin [a *], Meltem Alp [a], Ahmed Şeref [a]

[a] *Department of Metallurgical and Materials Engineering, Faculty of Engineering, Muğla Sıtkı Koçman University, Muğla, TURKEY*
** Corresponding author's e-mail address: erdemsahin@mu.edu.tr*
DOI: 10.29130/dubited.1371973

ABSTRACT

Rapid degradation in body fluids is known to be the main shortcoming of the AZ31 magnesium alloy that is aimed to be controlled in this study by chemical conversion of its surface in various phosphate and chloride solutions. Deposited layers on the surface of bare alloy plates were subjected to compositional and morphological analyses to assess their performance as barriers to degradation. Also changes in the mass of the samples and pH of the solutions were monitored during 21 day immersion periods. Formations of prismatic, platelike, needlelike crystals of various compositions including calcium phosphates, magnesium phosphates, magnesium chlorides were observed by scanning electron microscopy and their atomic compositions were determined by EDX and quantitative XRD analyses. The results indicate that a layer of ceramic of various thicknesses can stably form on the base alloy by simple adsorption of the particles suspended in the solution or by nucleation and growth of the products of reactions between dissolved ions and the metal ions released from the surface. These deposition layers that are solely induced by the electrochemical potential of the species in the solution offer facile surface modification methods and novel phases to control the degradation of magnesium alloys in aggressive environments such as body fluids or marine environments.

Keywords: *AZ31 magnesium alloy, Coating, Magnesium phosphates, Calcium phosphates, Phase analysis.*

Çeşitli Sulu Çözeltilerde Tutulan Magnezyum AZ31 Numunelerinin Yüzey Analizi

ÖZ

Vücut ortamında hızlı bozunduğu bilinen AZ31 magnezyum alaşım yüzeyinin bu eksikliğinin çalışmamızda çeşitli fosfat ve klorür çözeltilerinde kimyasal dönüşüme maruz bırakılarak giderilmesi amaçlanmıştır. Alaşım plakaların yüzeyinde biriken katmanlar bozunmaya karşı bariyer performanslarını değerlendirmek için kimyasal ve morfolojik analizlere tabi tutulmuştur. Ayrıca numunelerin kütlesindeki ve çözeltilerin pH'ındaki değişiklikler 21 günlük daldırma süreleri boyunca izlenmiştir. Kalsiyum fosfatlar, magnezyum fosfatlar, magnezyum klorürler gibi çeşitli bileşimlerdeki prizmatik, plakamsı ve iğnemsi kristal oluşumları taramalı elektron mikroskobu ile incelenmiş ve bunların atomik bileşimleri EDX ve kantitatif XRD analizleri ile belirlenmiştir. Sonuçlar alaşım üzerinde çeşitli kalınlıklarda bir seramik tabakasının, basit adsorpsiyon ve çözünmüş iyonlar ile yüzeyden salınan metal iyonları arasındaki reaksiyon ürünlerinin çekirdeklenmesi ve büyümesi yoluyla kararlı bir şekilde oluşabildiğini göstermektedir. Yalnızca çözeltideki türlerin elektrokimyasal potansiyeli ile oluşan bu birikim katmanları, vücut sıvıları veya deniz ortamları gibi agresif ortamlarda magnezyum alaşımlarının bozunmasını kontrol etmek için sade bir yüzey modifikasyon yöntemi ve yeni fazlar sunmaktadır.

Received: 06/10/2023, Revised: 04/12/2023, Accepted: 05/12/2023
Ulusal Elektron Mikroskopi Kongresi (EMK26)'nde sunularak özet metin olarak basılmıştır.

Anahtar Kelimeler: *AZ31 magnezyum alaşımı, Kaplama, Magnezyum fosfatlar, Kalsiyum fosfatlar, Faz analizi.*

I. INTRODUCTION

Inherently biocompatible magnesium (Mg) is a safe biomaterial that has ideal properties for non-load bearing maxillofacial applications except for its surface reactivity in contact with aqueous solutions. Various elements have been added to Mg matrix to improve its corrosion resistance and mechanical stability [1-5]. Mg and its alloys possess good specific strength and mechanical properties and biocompatibility behavior. The high strength/weight ratio [6] of Mg alloys make them attractive for widespread application including implantation *in vivo*. The degradation of Mg alloys is beneficial in hard tissue implants unlike steel or titanium implants which need second surgical operation to remove the implant. Controlled spontaneous degradation of Mg can mimic the tissue growth of bones and to deliver safe and nontoxic ions to the body [7-8].

AZXX family of Mg alloys are produced by incorporating aluminum, zinc and manganese for the purposes of improving the corrosion resistance, mechanical properties, and deformability. Still, rapid degradation in body fluids is found to be the main shortcoming of the AZ31 Mg alloys [9-11]. Hence, a rich literature on coating and converting Mg alloy surfaces has formed based on the motivation to improve their stability *in vivo*. Common strategies include coating with physically adsorbable inert suspensions of inorganic particles [12-13], grafting a chemically compatible reactive suspension [14], electrodeposition of an inert layer from solutions [15-17], sputtering with ceramic particles under high energy [18-19] and chemically converting the surface in reactive bath solutions [11, 20-21]. The hybrid approach between simple adsorption of aqueous suspensions, grafting and chemical conversion is an unexplored route with promising results as evident from the literature on coating of metallic implants with calcium phosphate and polymeric cements [2, 22-25]. Our approach focuses on such reactive coating layers, not for enhancing bonding with the bone tissue but to passivate the surface in contact with the body fluids. Such cementitious coatings on Mg alloys can be applied directly before implantation and let fully develop *in vivo* or they can be applied and dried up during the manufacturing stage, and continue development after the implantation by utilizing the body fluid as the solvent. The latter *in situ* approach offers a dynamically evolving surface microstructure that can beneficially counteract the natural biodegradation process that is detrimental to Mg based implants.

Coating of AZ31 surfaces with concentrated suspensions of multiple components that facilitate the desired in situ passivation mechanisms necessitates a detailed analysis of singluar and synergistic effects of the solute reagents. Solutions of NaCl and MgCl2 are known to disrupt the passivating hydroxide layer on the surface and help the transformation of the surface especially in alkaline solutions [5]. The pitting corrosion effect of chloride ions is aimed to be balanced by the dissolution inhibiting effect of the extra Mg2+ ions supplied by MgCl2. Samples immersed in NaCl solutions are known to develop Mg oxychloride phases with a porous structure of needle-like crystals. Here a more compact layer of Mg or calcium phosphates is aimed to replace oxychloride phases by supplying high concentrations of PO43- ions from the particles in coating suspension, similar to a cement reaction. Therefore AZ31 plates were tested in solutions of phosphate salts for their anticipated positive effect while chloride salts were employed for their adverse effects on surface stability. Initially the effects of single component solutions were investigated that provide a continuous supply of phosphate and chloride anions that are the precursors to Mg phosphate and Mg oxyxchloride cement products. The results provide a baseline reference for the subsequent studies on immersion in multiple component solutions and suspensions as a cementitious coating to control the degradation rate of Mg alloys.

II. MATERIAL AND METHODS

AZ31 alloys were cut into rectangular samples of around 2 cm^2 area and immersed in aqueous solutions of various compositions at ambient conditions (20 °C and atmospheric pressure). Alloy samples were placed statically in glass beakers with 200 mL of solutions for 21 days and analyzed at specific intervals (1, 3, 7, 14, 21 days) by gravimetry to account for the change in their mass. Also the solution pH was monitored at the same intervals. Test media included deionized water (DIW), 3.5 wt% NaCl, 3.5 wt% MgCl2 solutions and DIW saturated with phosphate salts: monocalcium phosphate (MCP), dicalcium phosphate (DCP), tricalcium phosphate (TCP), and potassium dihydrogen phosphate (PDP). All chemicals were commercially obtained analytical grade reagents. DIW was obtained from a Merck millipore Q3 machine. Immersion tests were completed after 21 days of monitoring the mass and pH variations. Extracted samples were dried in air at ambient conditions. The surfaces of the dried plates were characterized using SEM, EDX and XRD to identify the final composition.

Morphological analysis was done by using a FEI QUANTA 250 FEG scanning electron microscope. A secondary electron (SE) detector was used to capture micrographs at an accelerating voltage of 3.00 kV and a wedge distance of 10 mm. An electron dispersive X-ray detector coupled with a backscattered electron (BSE) detector was used for elemental analysis of the sample surface. The images were obtained at an accelerating voltage of 20 kV and a wedge distance of 5 mm. XRD analysis was conducted by using a Philips X'Pert Pro powder diffractometer with Cu Ka radiation at a generator voltage of 45 kV and a tube current of 40 mA. All XRD patterns were obtained at a scan step size of 0.05 and 4 seconds per step. Rietveld refinement method was employed for the quantitative XRD analysis. Profex software from Doebelin.org and XRD references from Crystallography Open Database were used for phase identification and quantification.

III. RESULTS AND DISCUSSIONS

The overall variation of sample weights in both aqua and aqueous solutions of single components is given in Figure 1. While DIW minimally affected the chemical stability of the alloy surfaces, they transformed gradually in all solutions. Generally calcium phosphate solutions resulted in relatively thinner depositions due to their lower solubility in water. Saturated PDP solution formed an especially thick layer which can be further compacted by the addition of various other phases. NaCl and MgCl2 solutions also resulted in a thick Mg oxychloride layer that is loose due to the needle-like crystal morphology. Therefore chloride salts should not be added to multiple component solutions in high concentrations, its amount should be kept at an optimum level for the purpose of activating the alloy surfaces in alkaline condition induced in DCP or TCP solutions.

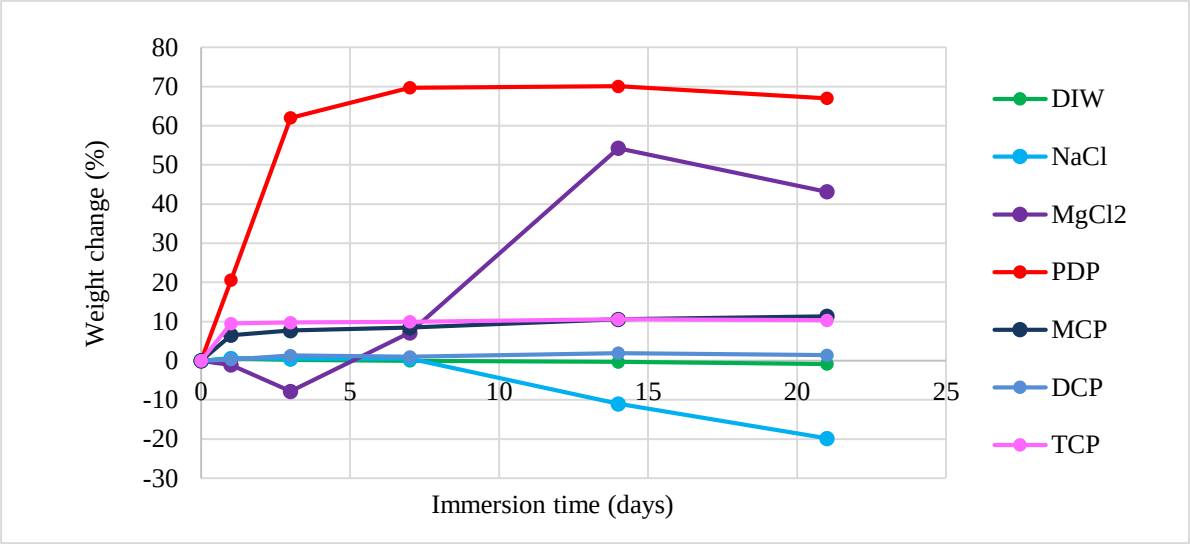

Figure 1. *Variation of the weight of samples immersed in solutions of single components with time.*

Variation of pH of the single phase solutions during immersion tests is given in Figure 2. The solutions were initially acidic in the presence of NaCl, PDP and MCP but all gradually became alkaline. It is an indication of early rapid dissolution of the surface, presumably at growing pits. Subsequent supersaturation build up of Mg hydroxide starts to passivate the surface gradually by the formation of either simple $Mg(OH)_2$ or more complex hydroxide compounds according to the species in the solution. In acidic MCP, NaCl and PDP solutions a passivating hydroxide layer cannot form on the surface of the alloys initially, rather Mg is exposed in a reactive form before transforming to products of reactions [5]. Chloride addition to these systems is not necessary due to their already reactive surfaces. Instead species that can slow down ion transport and dissolution like polymeric hydrogels and hydroxy carboxylic acid salts can produce a more controlled deposition.

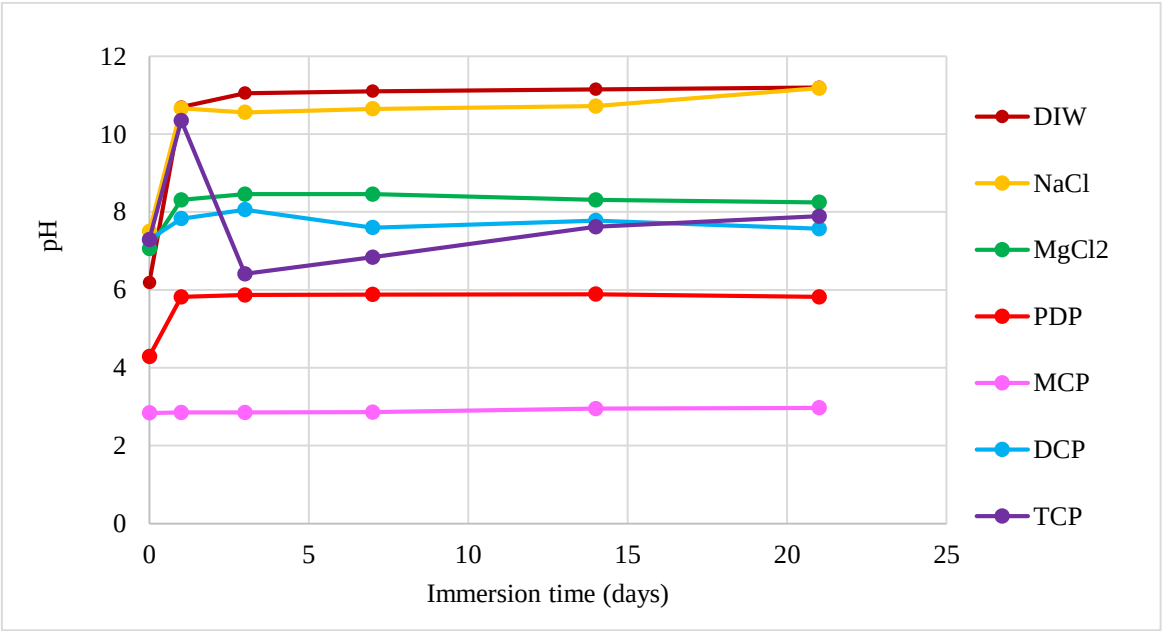

Figure 2. *Variation of solution pH in deposition systems containing single components.*

The degradation behavior of AZ31 in DIW serves as a baseline reference for other immersion tests. It is seen that the weight loss and depositions are negligible in pure water. According to the morphological and compositional analysis of these samples given in Figures 3 and 4, Mg metal and hydrotalcite

($Mg_6Al_2CO_3(OH)_{16}\cdot 4H_2O$,) were the detected phases on the surface of AZ31. As seen in Figure 4b, hydrotalcite peaks are broad and intense which indicates that these crystals are nanoscale and cover the surface uniformly. The BSE detector image in Figure 4a revealed the presence of bright spots that are homogeneously distributed on the surface. These inclusions that are also visible in Figures 3a and 3b, are composed of Mn, Zn, Al and Mg in some form of intermetallic compound that is oxidized as well, according to the point EDX analysis on one of them (spectrum 25). These are known to form during the alloying process and function as passivation points by binding elements that can cause micro-galvanic corrosion [26]. Figures 3c, 3d and 4a show that these phases form a microporous structure on the surface, that likely originates from the degradation of the grain boundaries of the elongated surface grains.

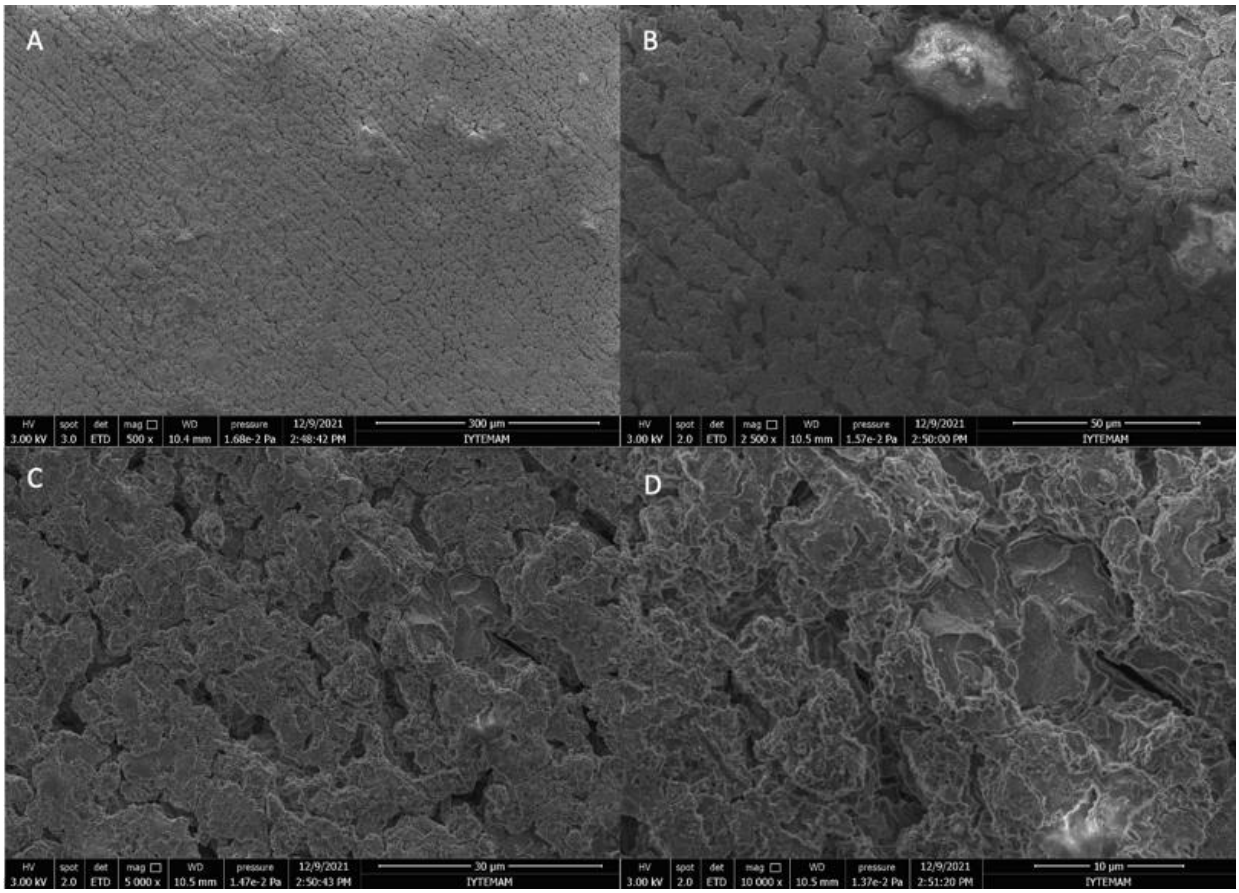

Figure 3. *Microstructure of AZ31 surfaces immersed in pure water, imaged using a SE detector at a magnfication of:* ***(A)*** *500x,* ***(B)*** *2500X,* ***(C)*** *5000X,* ***(D)*** *10000X.*

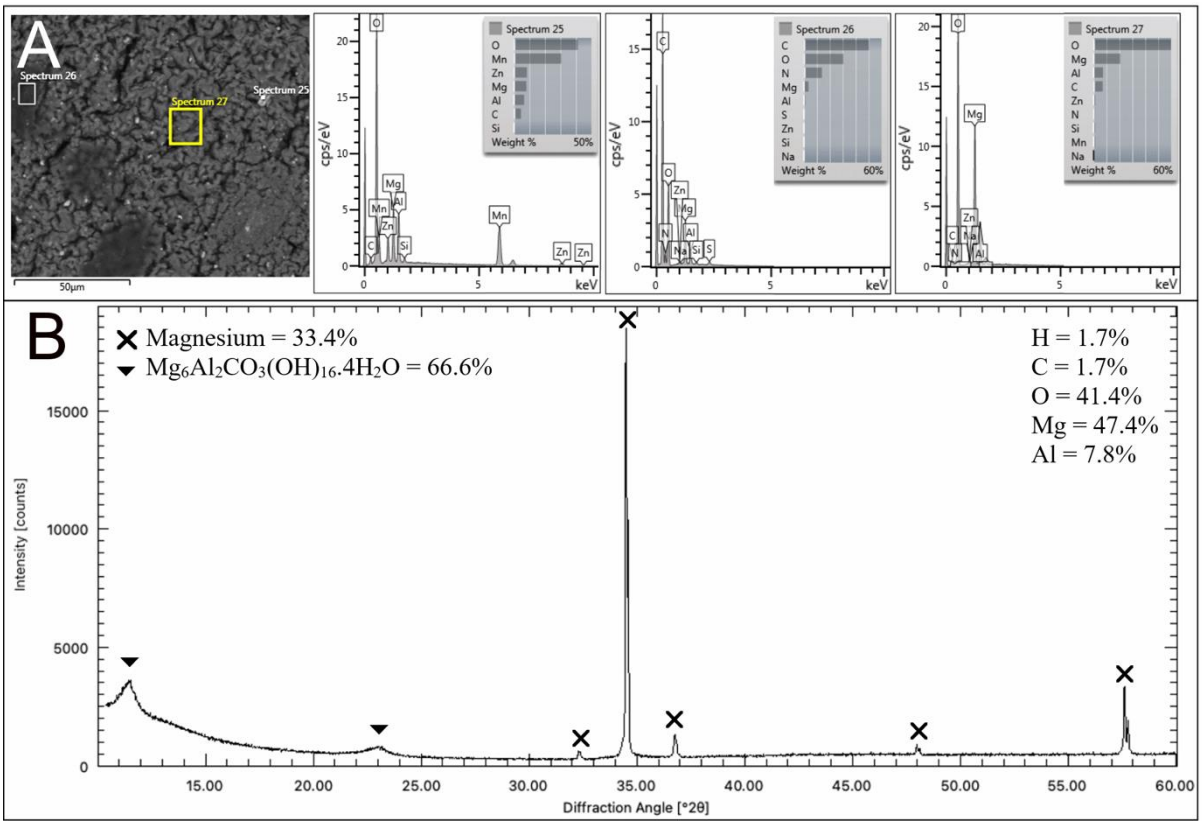

Figure 4. *Compositional analysis of AZ31 samples immersed in DIW for 21 days:* ***A)*** *EDX analysis results from an area imaged with a BSE detector (spectra depict weight ratios),* ***B)*** *Quantitative XRD analysis results (percentages of the compounds and elements are based on weight).*

It was observed that AZ31 rapidly degraded in NaCl solution with the formation of a thick Mg oxychloride layer. This is reflected in the morphological and phase analysis given in Figures 5e,f and 6a. Bush-like formations of oxychloride needles create loosely interpenetrating layers. MgO, Mg(OH)2 and various Mg oxychloride stoichiometry were detected by EDX analysis. The elemental ratio of Mg/Cl was found between 4 to 2 and Mg/O was found close to 1/3 in the needles which point to the formations of $5Mg(OH)_2 \cdot MgCl_2 \cdot 8H_2O$, also known as the 5-1-8 phase in Mg oxychloride cement literature. The higher ratio of Mg/O at region 8 indicates some of the X-ray signals are coming from deeper parts where Mg metal is present. These observations were further confirmed by quantitative XRD of the dry surfaces after deposition (Figure 6b). Mg was found in abundance and the rest of the surface (excluding gold coating) was 5-1-8 phase.

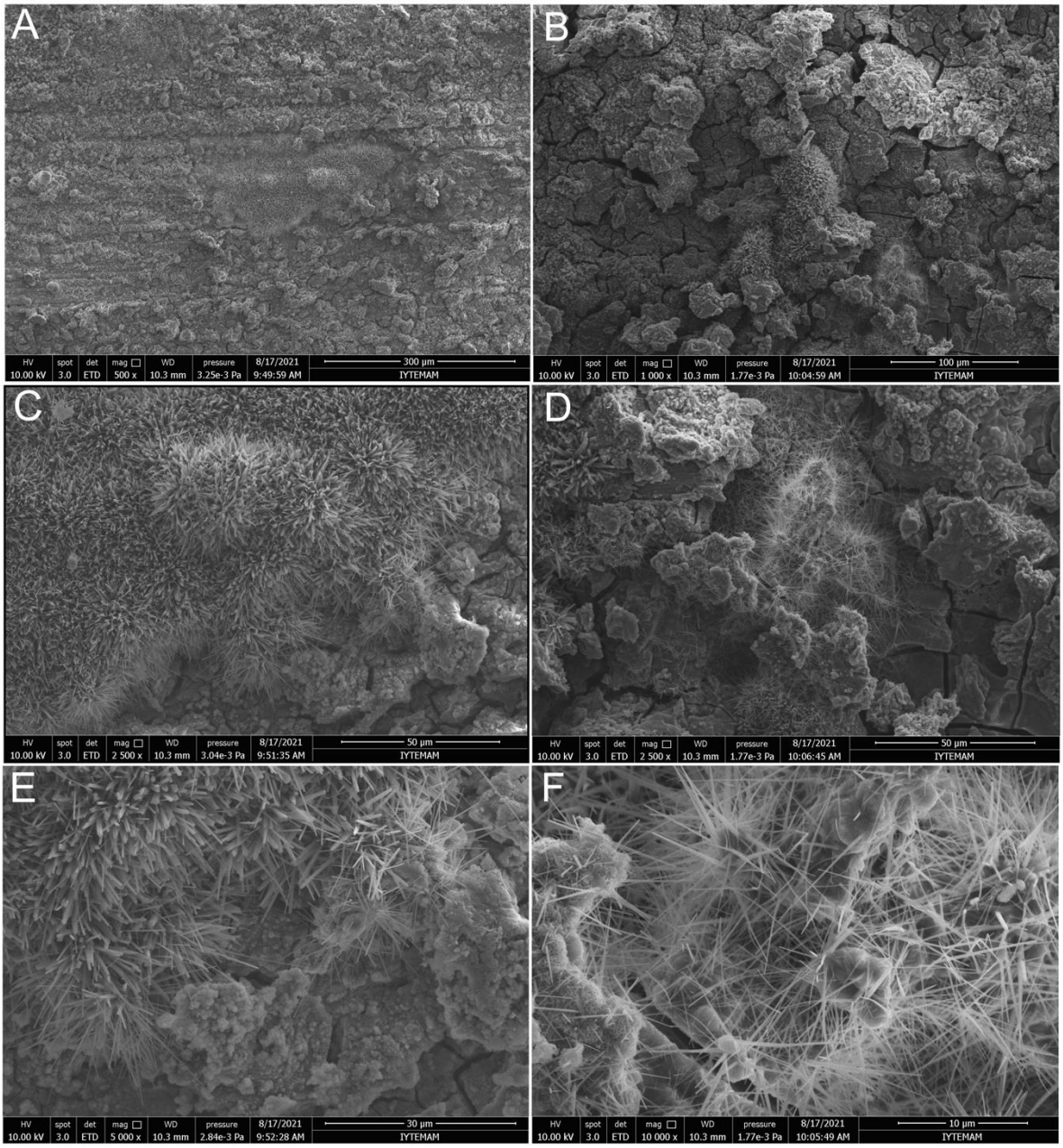

Figure 5. *Microstructure of AZ31 surfaces immersed in 3.5 wt% NaCl solution, imaged using a SE detector at a magnfication of:* ***(A)*** *500x,* ***(B)*** *1000X,* ***(C, D)*** *2500X,* ***(E)*** *5000X,* ***(F)*** *10000X.*

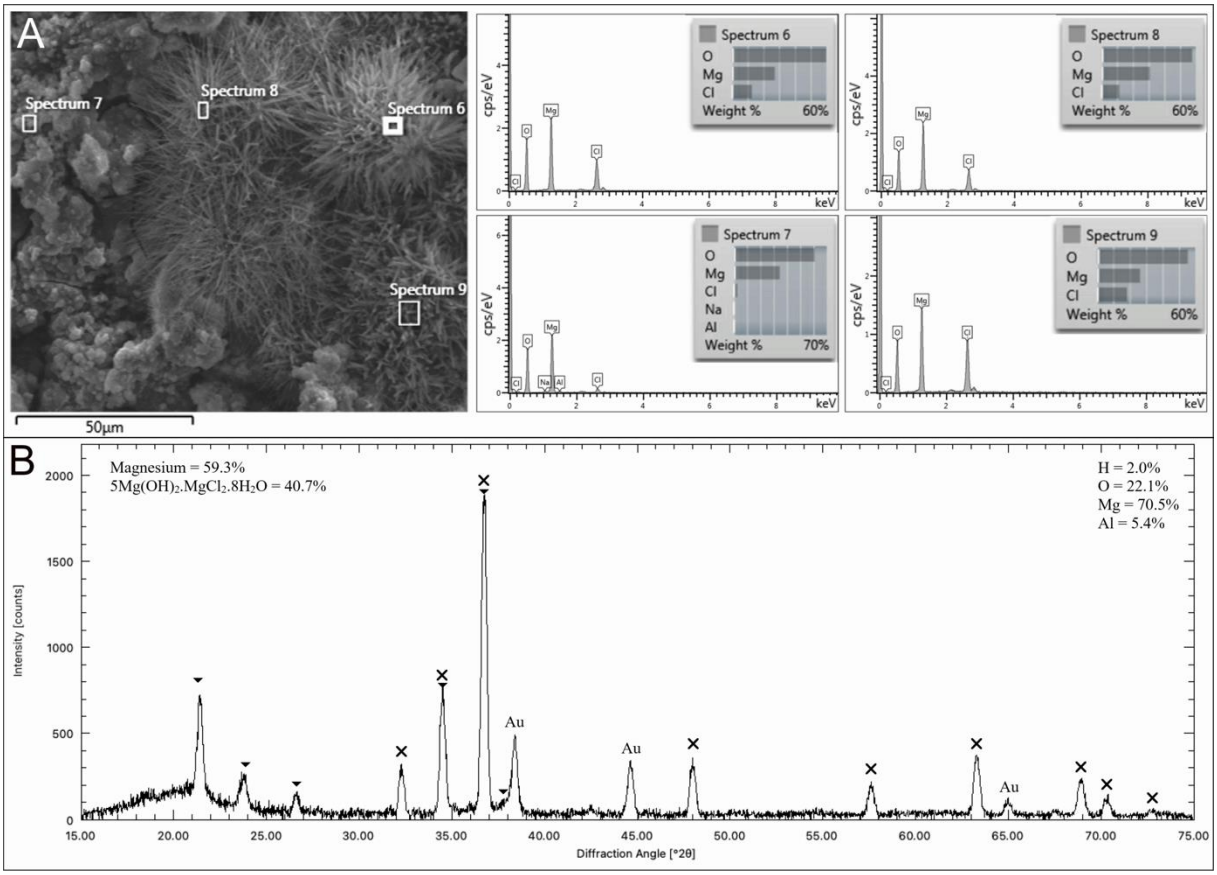

Figure 6. *Compositional analysis of AZ31 plate immersed in 3.5% sodium chloride solution:* ***A)*** *EDX analysis results from an area imaged with a BSE detector (spectra depict weight ratios),* ***B)*** *Quantitative XRD analysis results (percentages of the compounds and elements are based on weight).*

The effect of Mg chloride was also investigated by EDX and gravimetric analysis. The elemental composition given in Figure 7 shows similar stoichiometric ratios as the NaCl solution. The ratio of Mg/Cl was found around 3 in spectrum 1 while it was around 2 in the second and third regions. The O/Mg ratio in all three regions was around 4. The stoichiometry of regions 2 and 3 corresponds to 3-1-8 phase (3Mg(OH)2·MgCl2·8H2O) that is detected in XRD analysis to be around 11%. The stoichiometry obtained from region 1 is most likely the 5-1-8 phase that was also found on samples immersed in NaCl solutions. It is known to convert to $3Mg(OH)_2{\cdot}MgCl_2{\cdot}8H_2O$ and then to $2MgCO_3{\cdot}Mg(OH)_2{\cdot}MgCl_2{\cdot}6H_2O$ upon drying in air after the XRD analysis which explains the C peaks in the spectra. Close examination of these regions shows that there are characteristic needle structure of 5-1-8 around the tubular structure that is presumed to be 3-1-8 phase (Figure 8).

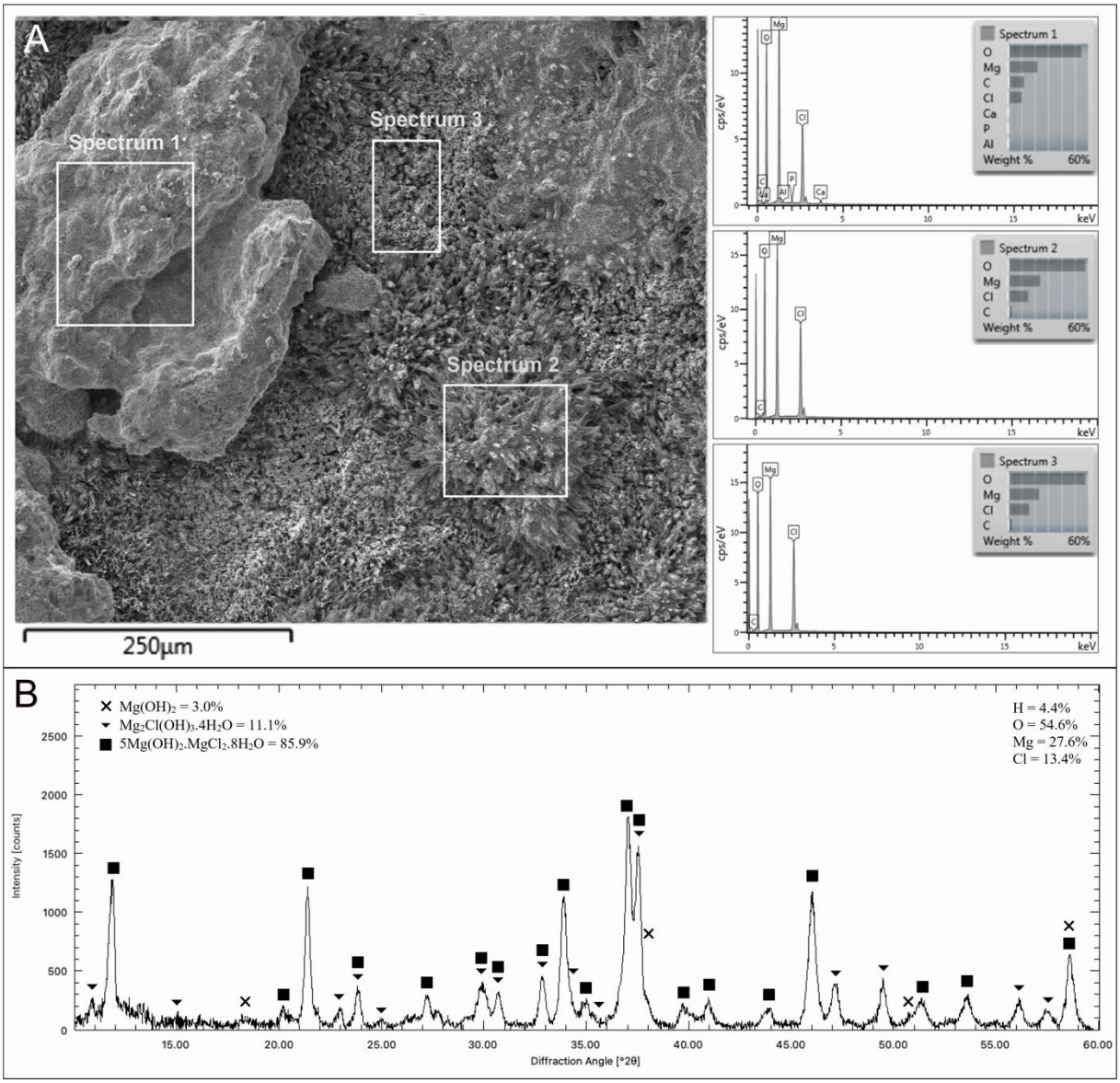

Figure 7*. Compositional analysis of AZ31 plate immersed in 3.5 wt% Mg chloride solution:* ***A)*** *EDX analysis results from an area imaged with a BSE detector (spectra depict weight ratios),* ***B)*** *Quantitative XRD analysis results (percentages of the compounds and elements are based on weight).*

The variation of sample weight upon immersion in 3.5 wt% Mg chloride and sodium chloride solutions shows a slight difference such that mass loss is detected in the first few days in Mg chloride solution that is followed by significant deposition up to day 14, while NaCl solution immediately caused deposition. There is a significant difference in the initial pH values between the two solutions which stems from higher initial Mg ion concentration and the resulting smaller chemical potential for dissolution in Mg chloride solution. The pH increase seen in Figure 2 for the initial period resulted from the dissolution of Mg hydroxides and the subsequent fall is attributed to the formation of the oxychloride phases.

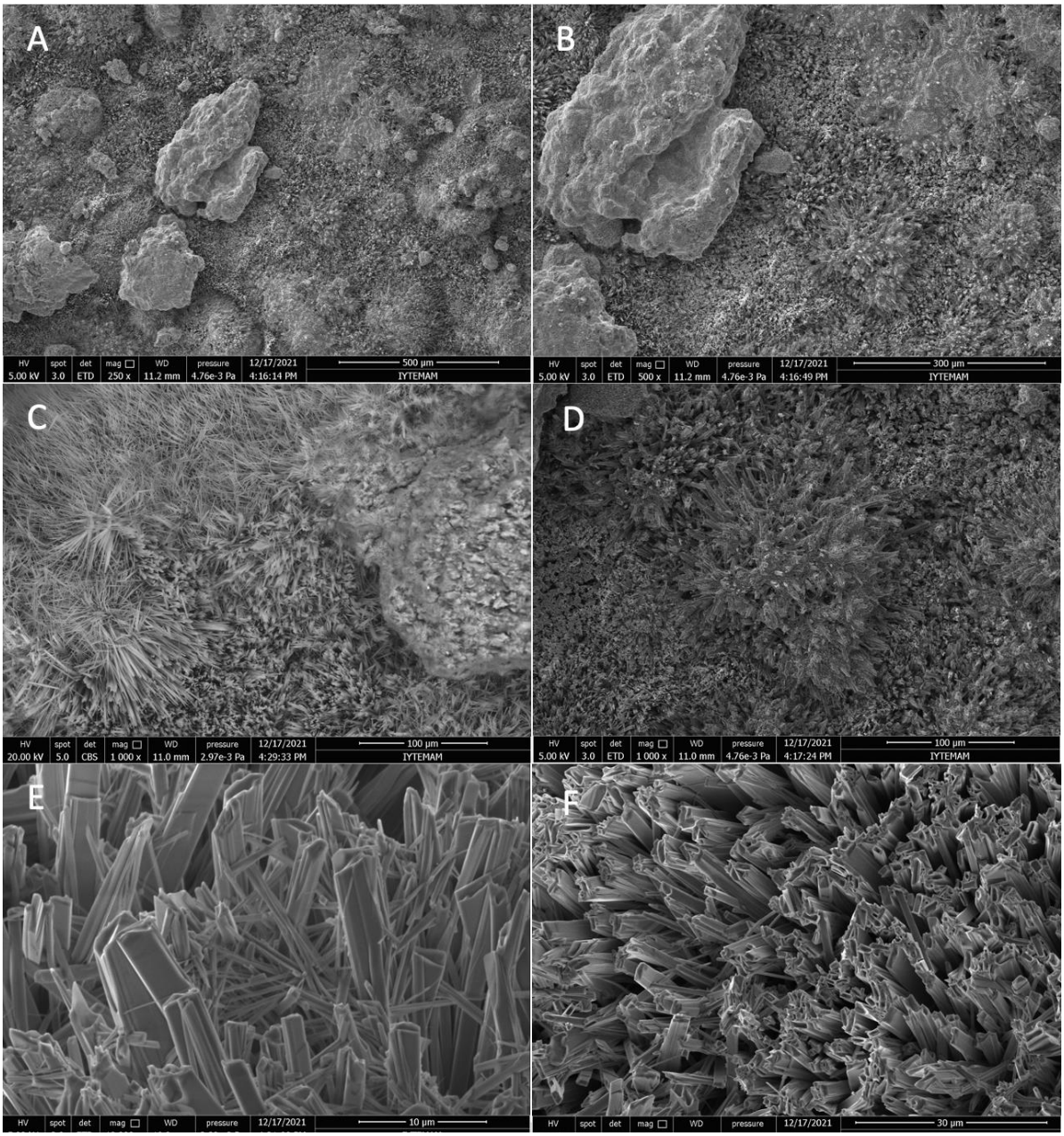

Figure 8. *Surface morphology of AZ31 sample immersed in saturated $MgCl_2$ solution for 21 days, imaged using a SE detector at a magnfication of: :* ***(A)*** *250X,* ***(B)*** *500X,* ***(C)*** *1000X,* ***(D)*** *1000X,* ***(E)*** *10000X,* ***(F)*** *5000X.*

The MCP solution is highly acidic and provides a favorable medium for the chemical conversion of Mg alloys. Figure 1 shows that a sudden deposition upon immersion was followed by gradual increase in weight. As a result the solution increased continuously from 2.84 to 2.97. According to phase analysis results, the acidic solution induced the formation of CaHPO4 and CaHPO4.2H2O phases that are stable under acidic conditions (Figure 9). Their Ca/P ratio of 1 is more than that of MCP (1/2) which requires some phosphate to stay in solution or to form a Mg phosphate compound. There are no Mg atoms or compounds on the surface according to the surface phase analysis. This is attributed to the inhibiting effect of the acidic medium on Mg hydroxide formation and the competition provided by calcium phosphates to acidic Mg phosphates such as newberyite. The detailed morphology shown in Figure 10 is compact with large calcium phosphate crystals that are characteristic of CaHPO4.2H2O [27].

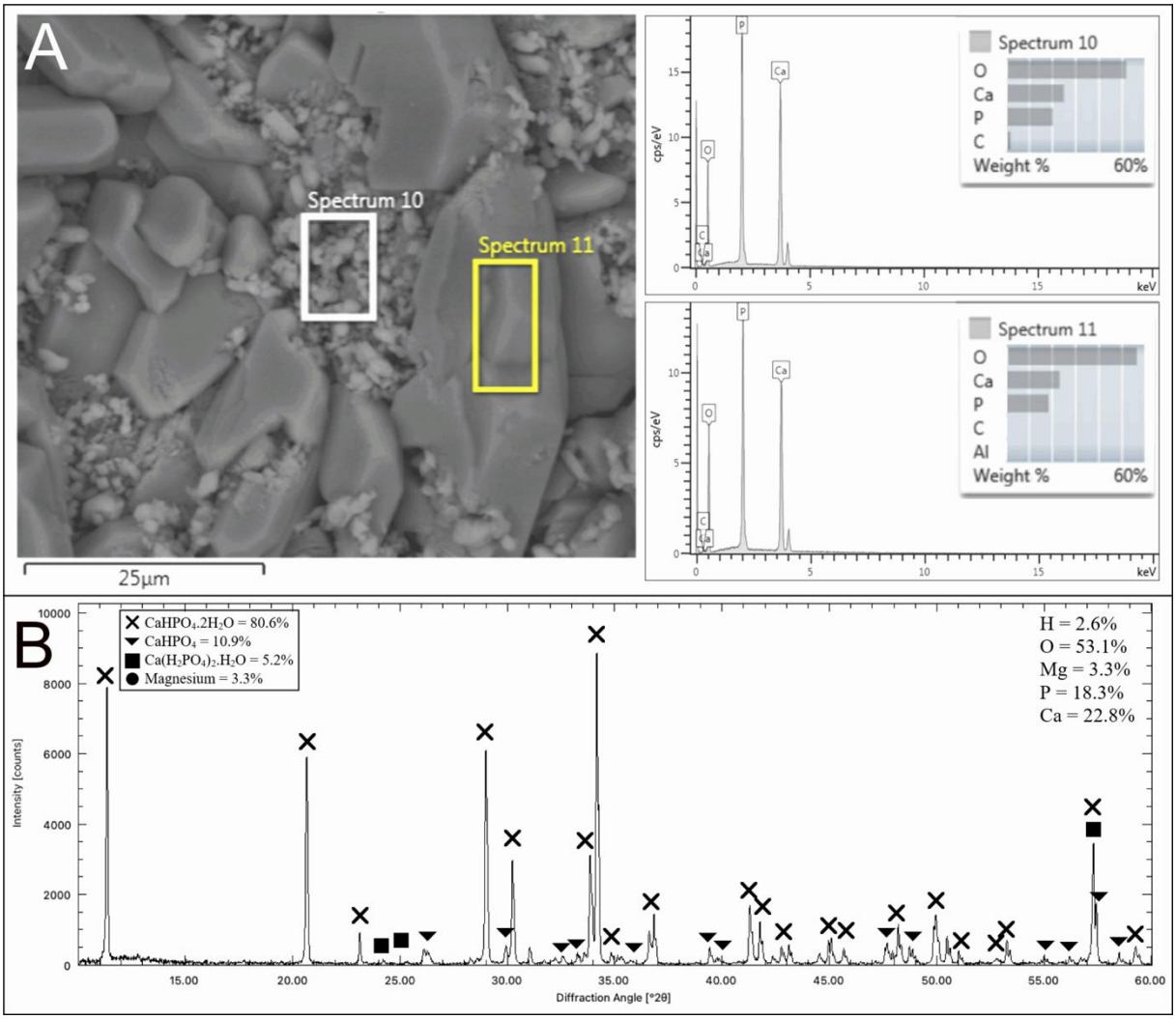

Figure 9. *Compositional analysis of AZ31 plate immersed in saturated MCP solution:* ***A)*** *EDX analysis results from an area imaged with a BSE detector (spectra depict weight ratios),* ***B)*** *Quantitative XRD analysis results (percentages of the compounds and elements are based on weight).*

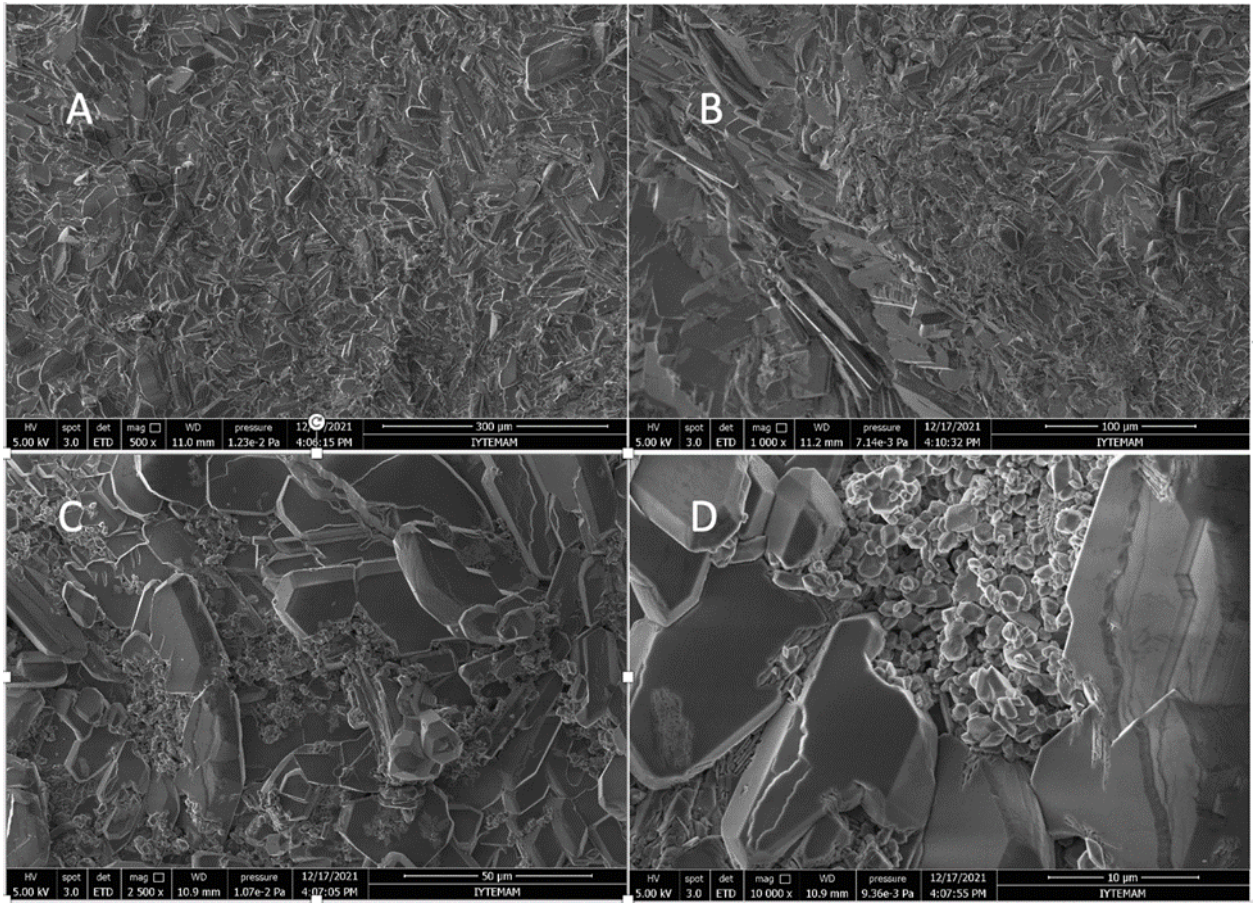

Figure 10. *Surface morphology of AZ31 sample immersed in saturated MCP solution for 21 days, imaged using a SE detector at a magnfication of:* ***(A)*** *500X,* ***(B)*** *1000X,* ***(C)*** *2500X,* ***(D)*** *10000X.*

The saturated solution of DCP contains less calcium and phosphate ions and is less acidic compared to the saturated MCP solution due to its much less solubility in water. As a result, the weight of the sample immersed in this solution only increased by 1% in 21 days. This was accompained by a parallel change in pH between 7.3-8.1. The surface analysis shows cracked layers of Mg hydroxide and phosphates that are covered with calcium phosphate particles (Figure 11). EDX spectra 8 and 9 reveal that the Ca/P ratio of these particles is around 1 (same as DCP). Therefore these particles are most likely physically adsorbed particles that were excess in solution. Spectrum 7 reveals that the cracked alloy surface contains some phosphate phase of Mg or aluminum, together with Mg hydroxides and carbonates that is stable at neutral pH. Close examination of the surface layer reveals that a sheet-like formation of these phases is present over the alloy surface (Figure 12). Its formation mechanism is thought to be a cementitious reaction, gradual dissolution of the deposited DCP particles in response to solution pH and integration of the phosphate anions with metal cations leaching from the surface. DCP phase is known to be stable at acidic conditions and transform to apatite as pH increases above neutral values [28]. The matching of the shapes of the broken pieces with the grain shapes indicates that they have grown epitaxially on the surface after the cracks have formed which should coincide with the second rise in the pH after14 days. Interestingly no phosphate compounds were found in XRD analysis as shown in Figure 11b. Only the base alloy and its hydroxide form was detected which means that the DCPD particles occupy a small proportion of the diffracting volume. The thin sheet layer may also be small compared to the alloy surface underneath or it may be a glassy phase that forms as a gel in the nanoscale. An intermetallic protrusion is also seen in Figure 12b.

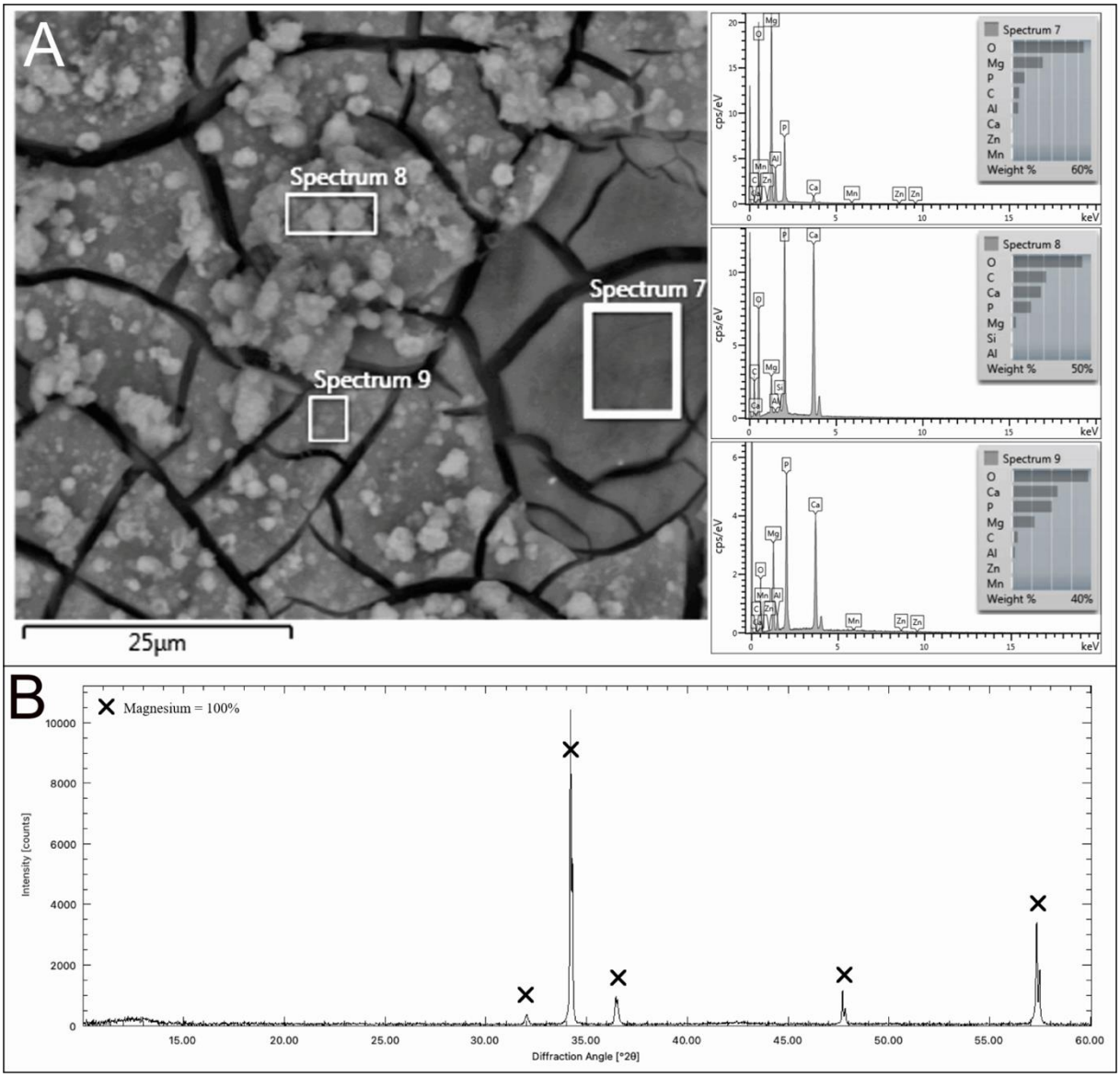

Figure 11. *Compositional analysis of AZ31 plate immersed in saturated DCP solution:* ***A)*** *EDX analysis results from an area imaged with a BSE detector (spectra depict weight ratios),* ***B)*** *Quantitative XRD analysis results.*

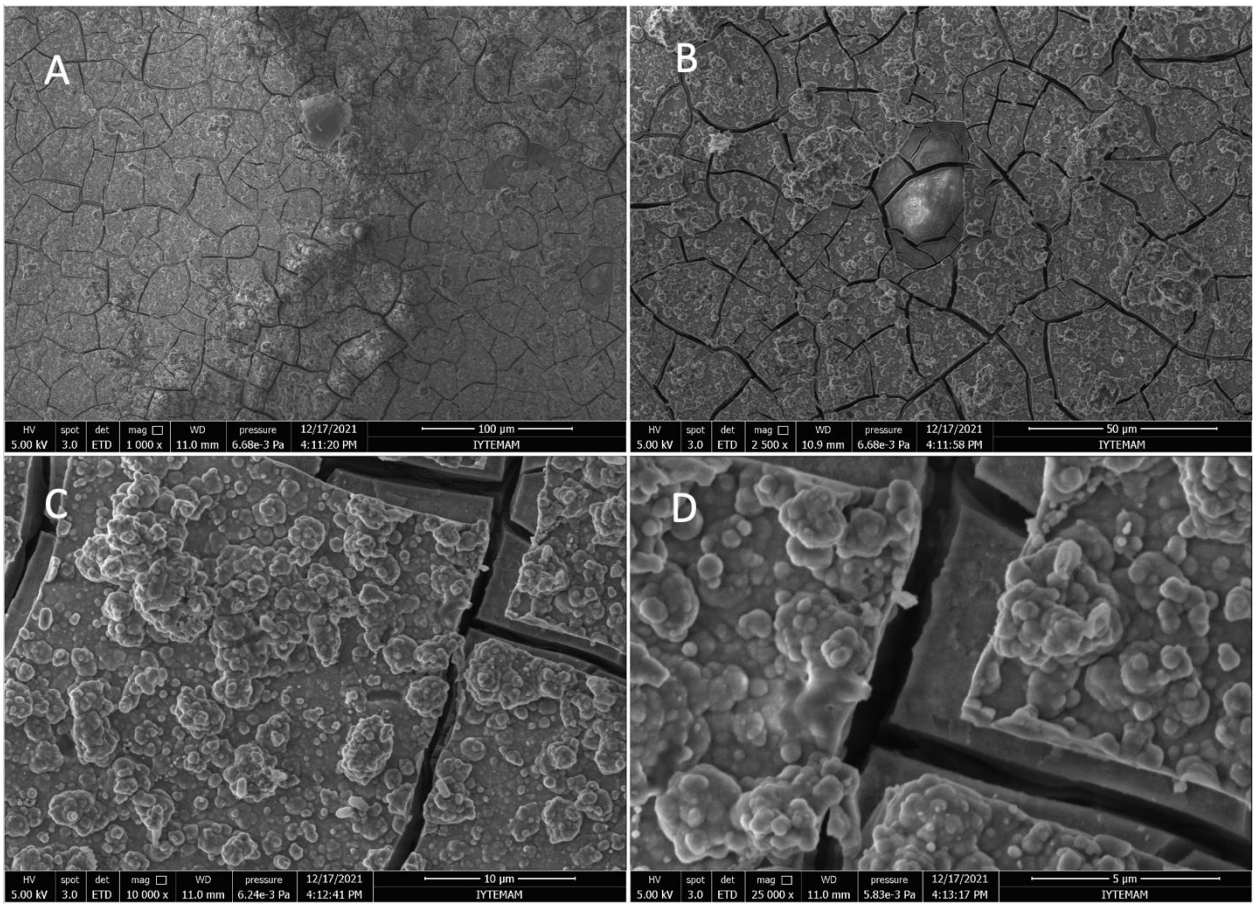

Figure 12. *Surface morphology of AZ31 sample immersed in saturated DCP solution for 21 days, imaged using a SE detector at a magnfication of:* ***(A)*** *1000X,* ***(B)*** *2500X,* ***(C)*** *10000X,* ***(D)*** *25000X.*

AZ31 plates immersed in TCP solution exhibited a sudden increase in weight in the first day but the weight remained relatively constant later (Figure 1). Solution pH fluctuated in a wide range between 6-10 during this abrupt change and then stabilized towards pH=8 (Figure 2). Unlike DCP, the TCP phase is stable under neutral and alkaline conditions but degrade rapidly under acidic conditions. For this reason, combination of MCP and TCP makes an effective bone cement with continuous dissolution of TCP under acidic conditions facilitated by MCP dissolution [28]. Aqueous TCP solution is inert by itself and this is reflected in the relatively constant weight and pH data after the first day. The initial rise in both data is assumed to be due to the covering of the surface by the physical adsorption of particles which may have caused some dissociation of hydrotalcite as well as TCP. EDX analysis of the surface shows that the particle agglomerations have a Ca/P atomic ratio between 1.4 and 1.7 which is close to the stoichiometric ratio of TCP (Figure 13a). Measurement on the bare surface yields a similar composition to the samples immersed in DCP solutions. Therefore the same sheet-like structure seems to be present here as well, with less concentrations of P, C, Al. This may be attributed to the more alkaline solution, smaller phosphate concentration supplied by TCP, less surface dissolution and less epitaxial formation on the hydrotalcite surface. Close examination shown in Figure 14 reveals that particle agglomerates have stably covered the surface. Unlike MCP and DCP, TCP can only form through solid state reactions at elevated temperature and the sintered morphology is its characteristic. XRD analysis of the alloy plate was essentially the same as that immersed in DCP solution (Figure 13b). Monolayers of physically adsorbed particles/agglomerates seem to be too thin for their detection by XRD and the bulk of the alloy plate diffracts at much more intensity. Their XRD pattern is simpler than the AZ31 alloy immersed in DIW, without the hydrotalcite peaks. Homogeneously covering hydrotalcite nanocrystals seem to be the precursor for the sheet structure formed with the physically adsorbed DCP and TCP.

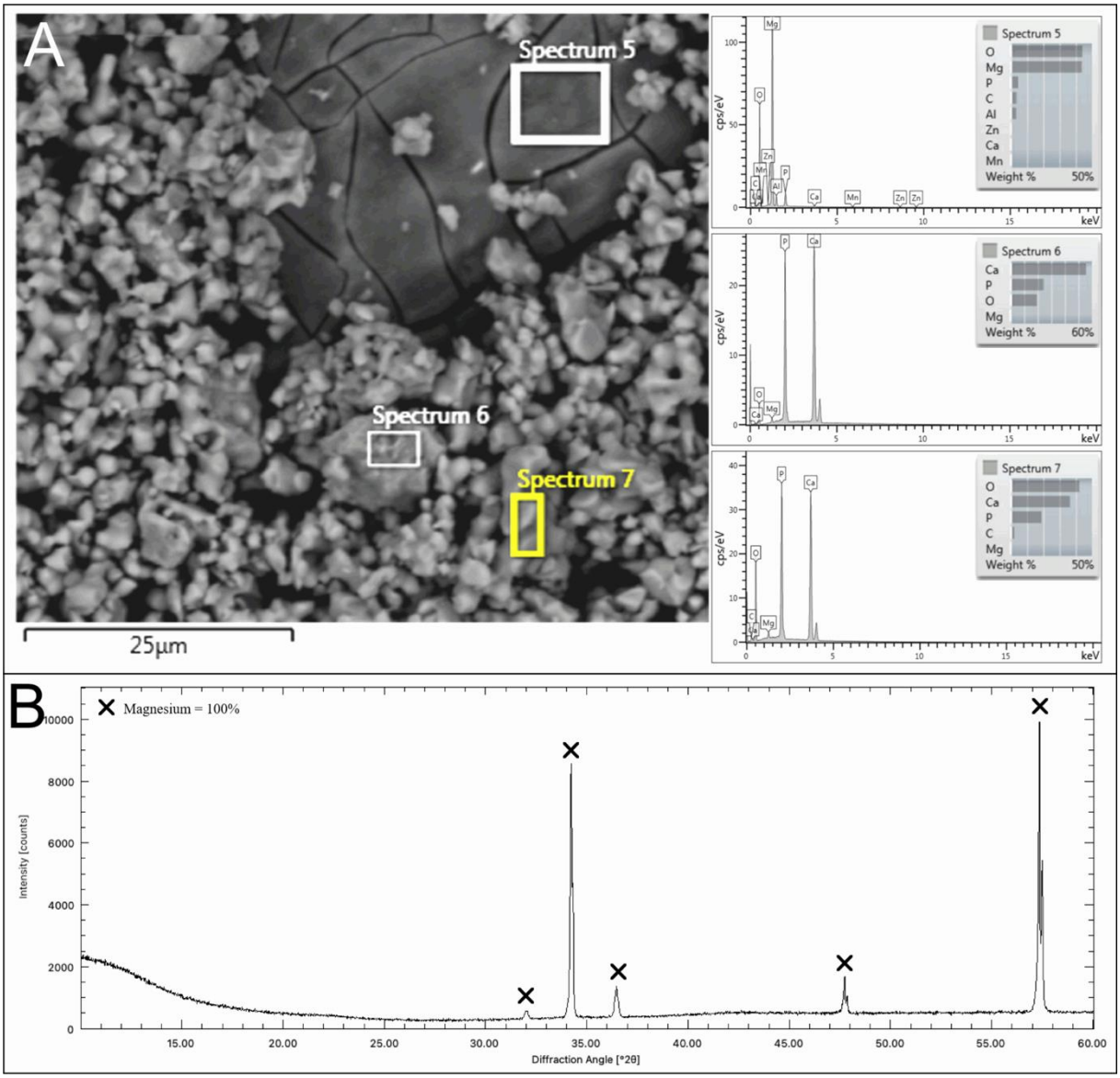

Figure 13*. Compositional analysis of AZ31 plate immersed in saturated TCP solution**: A)** EDX analysis results from an area imaged with a BSE detector (spectra depict weight ratios), **B)** Quantitative XRD analysis results.*

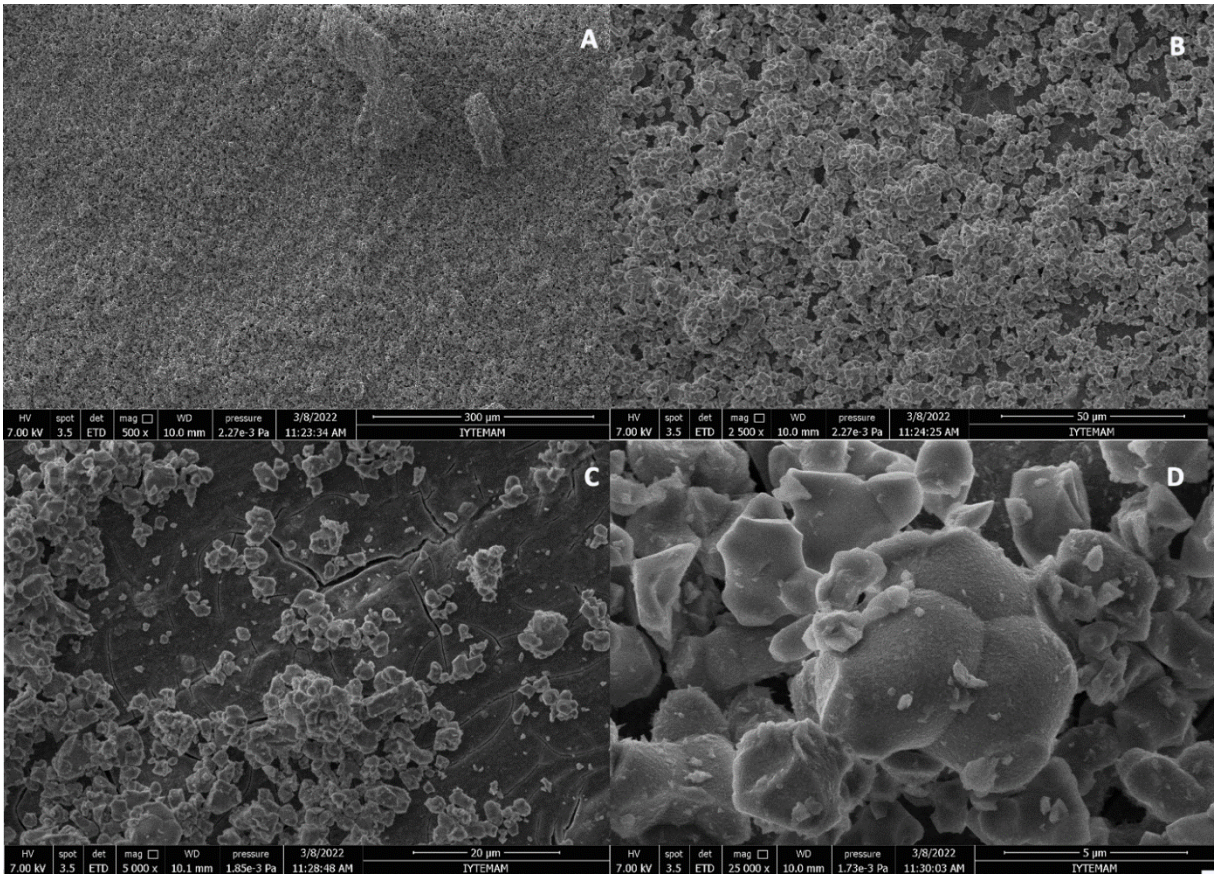

***Figure 14**. Surface morphology of AZ31 sample immersed in saturated TCP solution for 21 days, imaged using a SE detector at a magnfication of: **(A)** 500X, **(B)** 2500X, **(C)** 5000X, **(D)** 25000X.*

The saturated PDP solution is expected to form K-struvite (MgKPO4·6H2O) on Mg alloys under alkaline conditions and newberyite (MgHPO4·3H2O) under acidic conditions according to the Mg phosphate literature [29]. It induced a significant deposition in the first three days while the solution pH rose from 4 to 6 in the first day with no further changes in the remaining time. The surface analysis results reveal that a thick layer of newberyite deposited on the surface rather than K-struvite (Figure 15). K is only detected on the delaminated surface, possibly in struvite form as also found in XRD analysis. The thick layer consists of overlapped plates of newberyite according to the elemental ratios. Detailed surface morphology given in Figure 16 indicates a compact microstructure made of monolythic plates stacked next to each other.

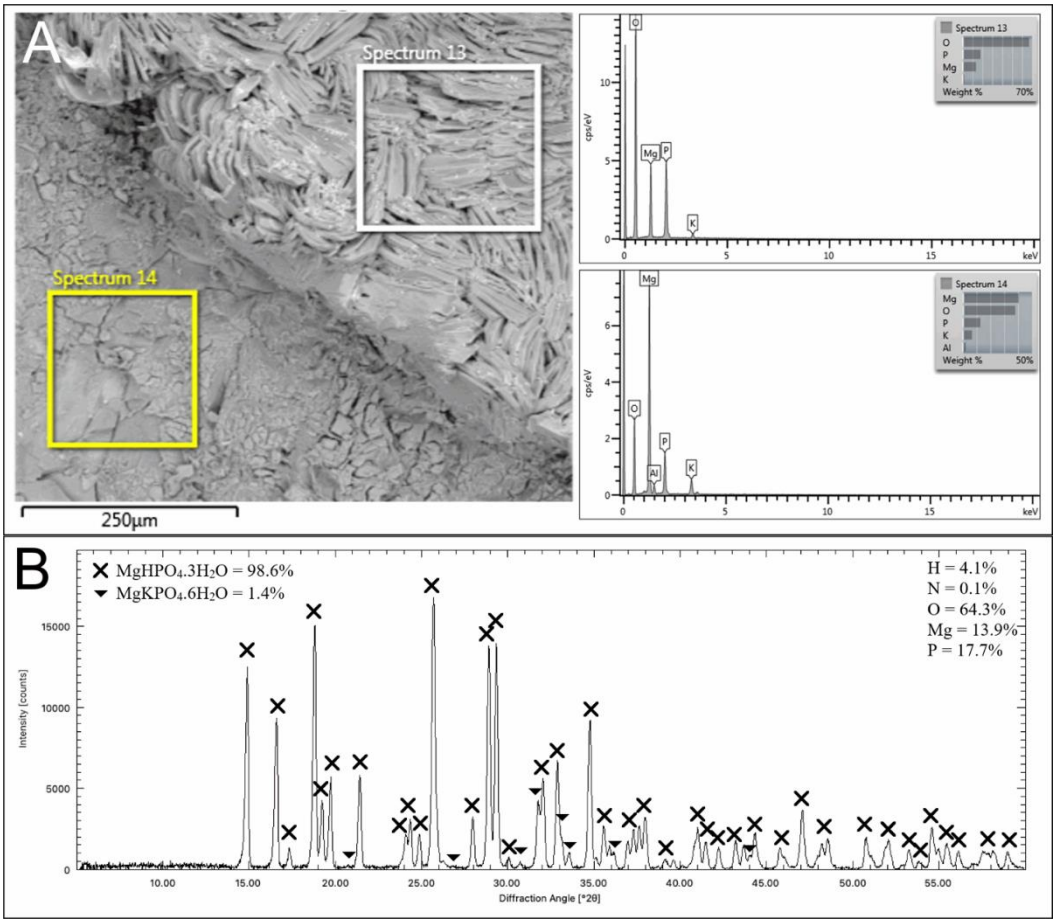

Figure 15. *Compositional analysis of AZ31 plate immersed in saturated PDP solution: A) EDX analysis results from an area imaged with a BSE detector (spectra depict weight ratios), B) Quantitative XRD analysis results (percentages of the compounds and elements are based on weight).*

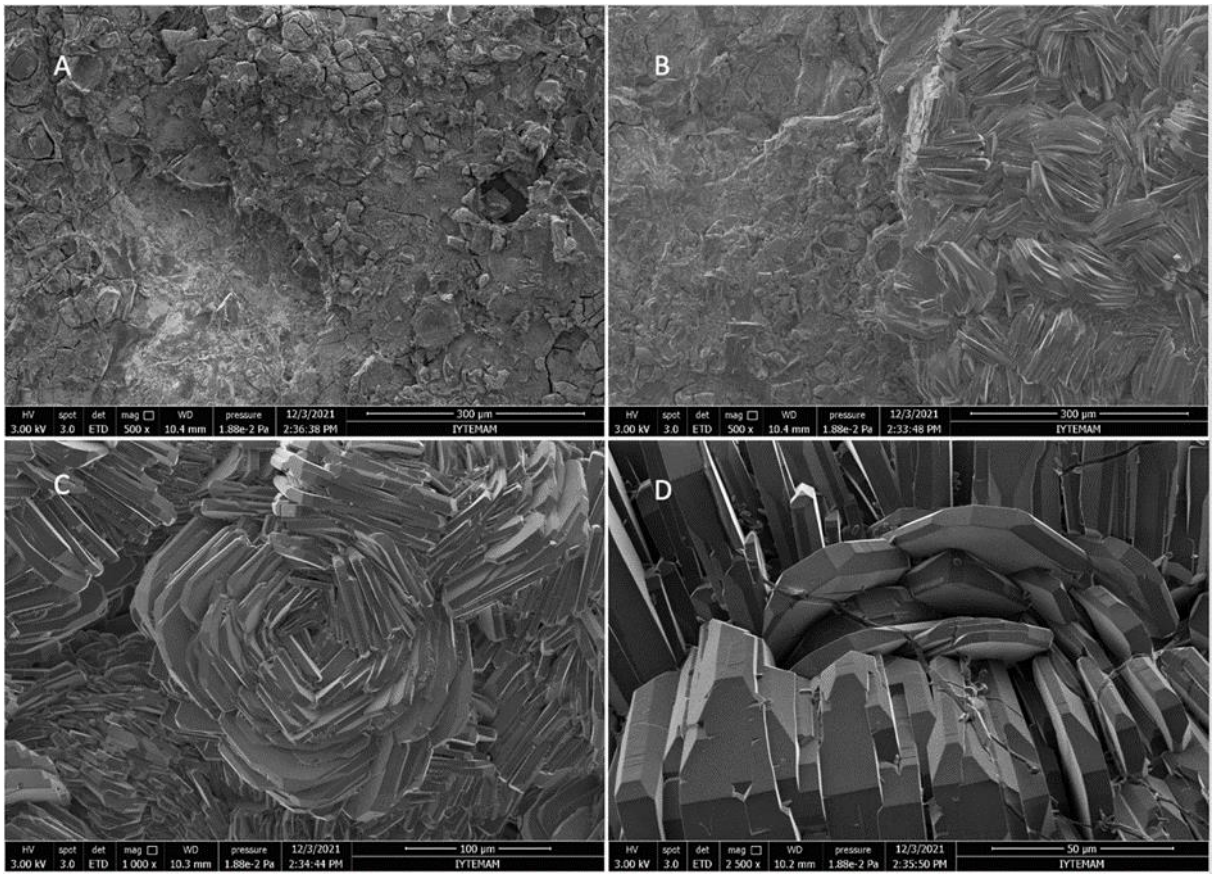

Figure 16. *Surface morphology of AZ31 sample immersed in saturated PDP solution for 21 days, imaged using a SE detector at a magnfication of: (A) 500X, (B) 500X, (C) 1000X, (D) 2500X.*

IV. CONCLUSION

AZ31 surfaces acquired compositions corresponding to the stoichiometries of Mg hydroxide carbonates, Mg phosphates and calcium phosphates upon immersing in various aqueous chloride and phosphate solutions. These are identified through EDX and XRD analyses as $Mg_6Al_2CO_3(OH)_{16}\cdot 4H_2O$ (hydrotalcite), $MgHPO_4.3H_2O$ (newberyite), $MgKHPO_4.6H_2O$ (struvite), $CaHPO_4.2H_2O$ (brushite or DCPD), $CaHPO_4$ (monetite or DCPA), $5Mg(OH)_2.MgCl_2.8H_2O$ (5-1-8 oxychloride phase) and $3Mg(OH)_2.MgCl_2.8H_2O$ (3-1-8 oxychloride phase). $Mg(OH)_2$ (brucite) is also detected in small quantities. Detected X-ray diffraction intensity of base Mg matrix was high in the case of thin and phyically adsorbed particles while reactive media like chloride and acidic phosphate solutions resulted in a thick layer inhibiting its detection. A thin, sheet-like formation that is assumed to be originating from hydrotalcite formed in DCP and TCP solutions and could not be detected by XRD probably due to it nanostructure. Mg oxychloride morphologies are needle-like clusters with loose structures that are nonideal for barrier performance while newberiyte and brushite phases form a dense layer on AZ31 alloy. Further studies are focused on coating with concentrated suspensions of these saturated solutions to induce in situ formation of the barrier layer in contact with such aqueous environments. Th initial results confirm their strong resistance against corrosion.

ACKNOWLEDGEMENTS: The authors appreciate the financial support from Scientific and Technological Research Council of Turkiye (TUBITAK) (Project No: 2020-119N759). İzmir Institute of Technology Materials Research Center staff is acknowledged for their assistance in characterizations. Doebelin.org and Crystallography Open Database (Crystallography.net) are acknowledged for sharing their XRD analysis software and database.

V. REFERENCES

[1] X. Li, X. Liu, S. Wu, K. W. K. Yeung, Y. Zheng, and P. K. Chu, "Design of magnesium alloys with controllable degradation for biomedical implants: From bulk to surface," *Acta Biomater.*, vol. 45, pp. 2–30, 2016.

[2] Z. Ran, W. Dai, K. Xie, and Y. Hao, "Advances of biodegradable magnesiumbased implants for orthopaedics," *Life Res.*, vol. 5, no. 7, pp.1-12, 2022.

[3] T. Cain, L. G. Bland, N. Birbilis, and J. R. Scully, "A compilation of corrosion potentials for magnesium alloys," *Corrosion*, vol. 70, no. 10, pp. 1043–1051, 2014.

[4] F. Witte, V. Kaese, H. Haferkamp, E. Switzer, A. Meyer-Lindenberg, C.J. Wirth, and H. Windhagen, "In vivo corrosion of four magnesium alloys and the associated bone response," *Biomaterials*, vol. 26, no. 17, pp. 3557–3563, 2005.

[5] F. Witte, N. Hort, C. Vogt, S. Cohen, K. U. Kainer, R. Willumeit, and F. Feyerabend, "Degradable biomaterials based on magnesium corrosion," *Curr. Opin. solid state Mater. Sci.*, vol. 12, no. 5–6, pp. 63–72, 2008.

[6] E. Ghali, "Magnesium and magnesium alloys," *Uhlig's Corros. Handb.*, pp. 809–836, 2011.

[7] W. D. Müller, M. L. Nascimento, M. Zeddies, M. Córsico, L. M. Gassa, and M. A. F. L. de Mele, "Magnesium and its alloys as degradable biomaterials: corrosion studies using potentiodynamic and EIS electrochemical techniques," *Mater. Res.*, vol. 10, pp. 5–10, 2007.

[8] Y. Xin, K. Huo, H. Tao, G. Tang, and P. K. Chu, "Influence of aggressive ions on the degradation behavior of biomedical magnesium alloy in physiological environment," *Acta Biomater.*, vol. 4, no. 6, 2008.

[9] S. Seetharaman, D. Sankaranarayanan, and M. Gupta, "Magnesium-Based Temporary Implants: Potential, Current Status, Applications, and Challenges," *J. Funct. Biomater.*, vol. 14, no. 6, p. 324, 2023.

[10] A. Carangelo, A. Acquesta, and T. Monetta, "Durability of AZ31 magnesium biodegradable alloys polydopamine aided. Part 2: ageing in Hank's solution," *J. Magnes. Alloy.*, vol. 7, no. 2, pp. 218–226, 2019.

[11] H. Hornberger, S. Virtanen, and A. R. Boccaccini, "Biomedical coatings on magnesium alloys–a review," *Acta Biomater.*, vol. 8, no. 7, pp. 2442–2455, 2012.

[12] Y. Wang, Z. Gu, J. Liu, J. Jiang, N. Yuan, J. Pu, and J. Ding., "An organic/inorganic composite multi-layer coating to improve the corrosion resistance of AZ31B Mg alloy," *Surf. Coatings Technol.*, vol. 360, pp. 276–284, 2019.

[13] Z. Q. Zhang, Y. X. Yang, J. A. Li, R. C. Zeng, and S. K. Guan, "Advances in coatings on magnesium alloys for cardiovascular stents–a review," *Bioact. Mater.*, vol. 6, no. 12, pp. 4729–4757, 2021.

[14] X. B. Chen, N. Birbilis, and T. B. Abbott, "Review of corrosion-resistant conversion coatings for magnesium and its alloys," *Corrosion*, vol. 67, no. 3, pp. 35001–35005, 2011.

[15] Y. Song, S. Zhang, J. Li, C. Zhao, and X. Zhang, "Electrodeposition of Ca–P coatings on

biodegradable Mg alloy: in vitro biomineralization behavior," *Acta Biomater.*, vol. 6, no. 5, pp. 1736–1742, 2010.

[16] J. H. Connor, W. E. Reid, and G. B. Wood, "Electrodeposition of metals from organic solutions: V. Electrodeposition of magnesium and magnesium alloys," *J. Electrochem. Soc.*, vol. 104, no. 1, p. 38, 1957.

[17] Q. Liu, D. Chen, and Z. Kang, "One-step electrodeposition process to fabricate corrosion-resistant superhydrophobic surface on magnesium alloy," *ACS Appl. Mater. Interfaces*, vol. 7, no. 3, pp. 1859–1867, 2015.

[18] L. Staišiūnas, P. Miečinskas, K. Leinartas, A. Selskis, A. Grigucevičienė, and E. Juzeliūnas, "Sputter-deposited Mg–Al–Zn–Cr alloys–Electrochemical characterization of single films and multilayer protection of AZ31 magnesium alloy," *Corros. Sci.*, vol. 80, pp. 487–493, 2014.

[19] G. Bikulčius, P. Miečinskas, A. Ručinskienė, A. Grigucevičienė, A. Selskis, and V. Pakštas, "Improvement of corrosion resistance of magnesium alloy by sputter coating with stainless steel," *Trans. IMF*, vol. 90, no. 3, pp. 125–128, 2012.

[20] A. R. Shashikala, R. Umarani, S. M. Mayanna, and A. K. Sharma, "Chemical conversion coatings on magnesium alloys-a comparative study," *Int. J. Electrochem. Sci.*, vol. 3, no. 9, pp. 993–1004, 2008.

[21] J. I. N. Hualan, Y. Xiangjie, and W. Ming, "Chemical conversion coating on AZ31B magnesium alloy and its corrosion tendency," *Acta Metall. Sin. (English Lett.*, vol. 22, no. 1, pp. 65–70, 2009.

[22] Y. Su, I. Cockerill, Y. Zheng, L. Tang, Y. X. Qin, and D. Zhu, "Biofunctionalization of metallic implants by calcium phosphate coatings," *Bioact. Mater.*, vol. 4, pp. 196–206, 2019.

[23] H. M. Wong, K. W. K. Yeung, K. O. Lam, V. Tam, P. K. Chu, K. D. K. Luk, and K. M. C. Cheung "A biodegradable polymer-based coating to control the performance of magnesium alloy orthopaedic implants," *Biomaterials*, vol. 31, no. 8, pp. 2084–2096, 2010.

[24] P. Tong, Y. Sheng, R. Hou, M. Iqbal, L. Chen, and J. Li, "Recent progress on coatings of biomedical magnesium alloy," *Smart Mater. Med.*, vol. 3, pp. 104–116, 2022.

[25] L. Y. Li, L. Y. Cui, R. C. Zeng, S. Q. Li, X. B. Chen, and Y. Zheng., "Advances in functionalized polymer coatings on biodegradable magnesium alloys–A review," *Acta Biomater.*, vol. 79, pp. 23–36, 2018.

[26] Y. Chen, Z. Xu, C. Smith, and J. Sankar, "Recent advances on the development of magnesium alloys for biodegradable implants," *Acta Biomater.*, vol. 10, no. 11, pp. 4561–4573, 2014.

[27] E. Şahin and M. Çiftçioğlu, "Monetite promoting effect of citric acid on brushite cement setting kinetics," *Mater. Res. Innov.*, vol. 18, no. 3, pp. 138–145, 2014.

[28] E. Şahin, "Calcium phosphate bone cements," in *Cement Based Materials*, London, United Kingdom, IntechOpen, 2018 vol. 191, pp. 191-219.

[29] E. V Musvoto, M. C. Wentzel, and G. A. Ekama, "Integrated chemical–physical processes modelling—II. simulating aeration treatment of anaerobic digester supernatants," *Water Res.*, vol. 34, no. 6, pp. 1868–1880, 2000.